AAPS PharmSciTech, Vol. 18, No. 5, July 2017 (© 2017)
DOI: 10.1208/s12249-016-0702-0

Research Article

Theme: Preparation of Nano and Micro-structures for Drug Delivery
Guest Editors: Dr. Z Ahmad and Prof. M Edirisinghe

Effect of Microneedle Type on Transdermal Permeation of Rizatriptan

Chandrateja Uppuluri,[1] Ashraf Sultana Shaik,[1] Tao Han,[2] Atul Nayak,[2] Karthik J. Nair,[3] Benjamin R. Whiteside,[3] Buchi N. Nalluri,[1,4] and Diganta B. Das[2,4]

Received 29 August 2016; accepted 21 December 2016; published online 11 January 2017

Abstract. The present study was aimed to investigate the effect of salient microneedle (MN) geometry parameters like length, density, shape and type on transdermal permeation of rizatriptan (RIZ). Studies were carried out using two types of MN devices *viz.* AdminPatch® arrays (ADM) (0.6, 0.9, 1.2 and 1.5 mm lengths) and laboratory-fabricated polymeric MNs (PMs) of 0.6 mm length. In the case of the PMs, arrays were applied three times at different places within a 1.77-cm^2 skin area (PM-3) to maintain the MN density closer to 0.6 mm ADM. Histological studies revealed that PM, owing to their geometry/design, formed wider and deeper microconduits when compared to ADM of similar length. Approximately 4.9- and 4.2-fold increases in the RIZ steady-state flux values were observed with 1.5 mm ADM and PM-3 applications when compared to the passive studies. A good correlation between different dimensionless parameters like the amount of RIZ permeated (C_t/C_s), thickness (h/L) and surface area (S_a/L^2) of the skin was observed with scaling analyses. Numerical simulations provided further information regarding the distribution of RIZ in MN-treated skin after application of different MNs. Overall, the study suggests that MN application enhances the RIZ transdermal permeation and the geometrical parameters of MNs play an important role in the degree enhancement.

KEY WORDS: histological sections; microneedle geometry; microneedles; numerical simulations; rizatriptan; scaling analyses; transdermal enhancement.

INTRODUCTION

Transdermal drug delivery (TDD) offers many advantages over conventional oral or injection delivery methods, for example, avoidance of hepatic first-pass metabolism, non-invasive nature of drug application, ability to deliver the drugs over a prolonged period of time, *etc*. All of these factors contribute to improved patient compliance and acceptability of drug therapy. TDD is gaining a lot of interest as a possible alternative route of administration for a wide array of therapeutic agents (1–3).

However, the greatest bottleneck with transdermal delivery is that only a limited number of drug molecules with a precise combination of physicochemical properties can permeate through the skin at clinically relevant/effective levels. The protective function of the skin, especially the outermost layer comprised of dead skin cells, the stratum corneum (SC), which is only 10 to 50 μm thick, imposes limitations on the drug molecules to permeate across the skin and to reach the systemic circulation. However, with the advent of research in TDD, several techniques have been proposed to attenuate or bypass the barrier function of the skin enabling the efficient delivery of drugs (3–6).

Migraine is a chronic, debilitating headache prevalent in about 19% of the global population with 2–3 times more incidence in women than in men (7). Rizatriptan, commonly available as benzoate salt (RIZ), an anti-migraine agent, is available as oral immediate release (IR) and oral disintegrating tablet (ODT) formulations, with an absolute bioavailability of about 45%. Moreover, with these formulations, a good chance of therapeutic failure within 2 h after administering the first dose and recurrence of the attack within 24 h was

[1] Department of Pharmaceutics, KVSR Siddhartha College of Pharmaceutical Sciences, Vijayawada, 520010, AP, India.
[2] Department of Chemical Engineering, Loughborough University, Loughborough, LE11 3TU, UK.
[3] Department of Engineering and Informatics, University of Bradford, Bradford, BD7 1DP, UK.
[4] To whom correspondence should be addressed. (e-mail: buchinalluri@yahoo.com; D.B.Das@lboro.ac.uk)

reported (8,9). Transdermal delivery may be seen as a good non-invasive alternative for RIZ administration with prolonged duration of action, increased bioavailability, reduced recurrence and increased patient compliance. However, RIZ is a relatively hydrophilic molecule and does not have ideal properties to permeate through the skin. Hence, a suitable permeation enhancement technique should be employed to achieve clinically significant rates of drug permeation.

Microneedles (MN), a novel transdermal permeation enhancement technique, are minimally invasive and potentially painless method of overcoming the barrier properties of the skin for enhanced delivery of drugs (6). This technique has many advantages when compared to hypodermic injection, is believed to make conduits of micrometre dimensions in skin layers in the epidermal layers (especially, SC) and thus believed to enhance the transdermal permeation of drugs (10). MNs are known to improve the permeation of drug molecules, including macromolecules like insulin, growth hormone, *etc.* (5,11–13). It has been reported in the literature that several geometric parameters of MNs like shape, dimensions, density of MN on the device and type, *etc.* play important roles in enhancing the transdermal permeation of drugs (14). There is also an interplay of the effect of these variables, and as such, their effects on the permeation of a drug molecule are generally non-intuitive. As a result, their effects are best studied for specific case.

Motivated by this idea, the present study was designed as a systematic approach to explore the effect of MN geometry on the extent of RIZ transdermal permeation enhancement. Two types of MN devices *viz.* commercially available AdminPatch® arrays (ADM) (0.6, 0.9, 1.2 and 1.5 mm length) and laboratory-fabricated polymeric MN arrays (PM) (0.6 mm length) of different MN densities were employed in this investigation (Fig. 1). A number of different techniques like etching, lithography and moulding were discussed widely in the literature for the manufacture of MNs of different dimensions (100–1800 μm in length) and shapes with different materials (plastics, silicon, ceramics, metals, *etc.*). Injection moulding offers several advantages in terms of ease of scalability for bulk manufacture, range of materials and good reproducibility (15). In this study, microinjection moulding was employed for the fabrication of PM arrays using polyether ether ketone (PEEK LT-3) as reported in a previous paper (16).

Surface visualization and histological evaluation of skin samples were carried out to confirm and to study formation microconduits by application of either types of MN devices. Moreover, the obtained RIZ permeation data was subjected to mathematical treatment using scaling analyses to obtain correlations between dimensionless parameters like amount of RIZ permeated (C_l/C_s) and various variables of the study like surface area (S_a/L^2) and thickness (h/L) of skin based on the principles of Buckingham π theorem as described in previous papers (17,18). Furthermore, numerical simulations using passive diffusion coefficient values, based on histological section images, were carried out using MATLAB and COMSOL programs in order to gain insights into the phenomenon of RIZ transport behaviour and distribution in the skin layers (18,19).

MATERIALS AND METHODS

Materials

AdminPatch® MN arrays were purchased from AdminMed, Sunnyvale, USA. Rizatriptan benzoate was obtained from Mylan Laboratories Limited, Hyderabad, India; sodium chloride, isopropyl alcohol, propylene glycol and 1% *w/v* safranin solution were from Loba Chemie, Mumbai, India; formic acid, acetonitrile, methanol and HPLC water from Merck Specialities Pvt. Ltd, Mumbai, India; and haematoxylin and eosin stain from Sigma-Aldrich, Bengaluru, India. All the reagents and chemicals used in the study were of HPLC grade. Pig ear skin was obtained from local abattoirs.

Fabrication of Polymeric MN

Moulding of the MNs was performed on a micropower 15 microinjection moulding machine as shown in Fig. 2a. It is the latest micromoulding machine from Battenfeld (Wellingborough, UK) and was employed for the fabrication of PM for its high repeatability, accurate dosing, clean room facility, *etc.*, which is ideal for the bulk manufacture of MNs. PEEK LT-3 is an FDA-approved semi-crystalline biomaterial manufactured by Invibio Inc, Lancashire, UK, and is widely employed for medical use. The main features of PEEK LT-3 include its excellent processability, dimensional stability and high mechanical performance and resilience to repeated gamma radiation and was hence selected for the fabrication of MN arrays (16). The MN mould insert (Fig. 2b) was made out of Stavax ESR (Bohler-Uddeholm Corp, Elgin, USA). Sink electrical discharge machining (EDM) was used to create negative MN features into the insert and was outsourced to Isometric Tool and Design Inc. (New Richmond, USA). The moulding parameters for PM were mentioned in Table I.

MN Dimensional Evaluation

Scanning Electron Microscope

A Hitachi TM-3000 table-top Scanning Electron Microscope was used for the analysis of the MN insert and needle geometry. The Hitachi TM-300 has a magnification from ×15 to ×30,000 and a sample chamber of 700 mm diameter and 50 mm thickness. It features 5 and 15 kV and analysis observation modes. Because of the high aspect ratio and low contrast of the MNs, analysis mode was used for imaging. The major advantage of using TM-3000 SEM was that it works under low vacuum and does not need specimen coating.

Confocal Laser Microscope

It is very important to measure the tip radius and height of the MNs, and the most common methods used are optical or electron microscopy. Because of its steep and complex

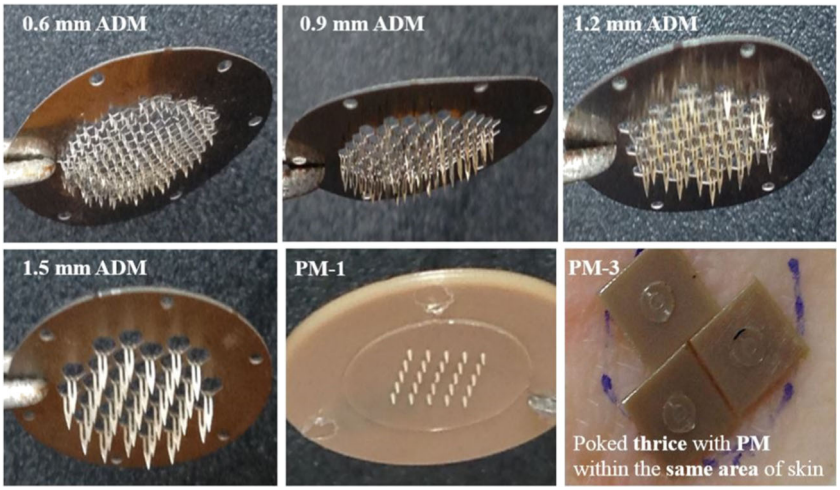

Fig. 1. Different MNs used in the study

structures, a 3D image analysis gives a better measurement of the needle geometry and quality control. In this study, an Olympus vertical scanning laser confocal microscope LEXT OLS 4000 was used to accurately measure the tip radius and height of MN arrays.

The device offers a broad magnification range from ×108 to ×17,280 and the exact 3D reconstruction of the MNs. The confocal laser microscope LEXT scans the surfaces with a laser beam with the wavelength of 405 nm thus allowing submicron visualization of material and component surfaces with the resolution of down to 0.10 μm. Measurements were taken with the ×20 lens using the wide range stitching feature with 20% overlap to produce a measurement area of 5 × 5 mm. A five-level brightness switch (Table II) was enabled to accurately illuminate the specimen.

Analysis of the Samples

The RP-HPLC-PDA method was developed specifically for the analysis of RIZ in the transdermal permeation samples. A Shimadzu Prominence HPLC system provided with DGU-20A3 degasser, LC-20AD binary pumps, SIL-

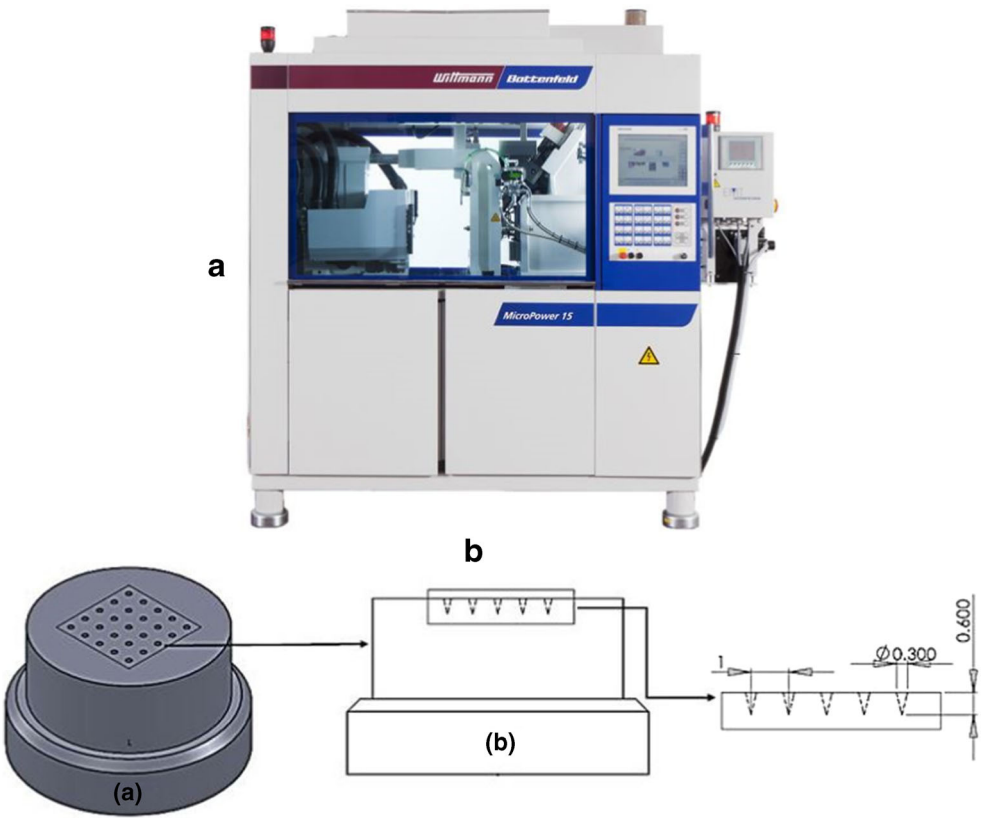

Fig. 2. **a** Battenfeld micropower 15 moulding machine. **b** *a* 3D drawing of the microneedle insert and *b* dimensions of the insert created using Solid-works CAD software (dimensions are in mm)

Table I. Microinjection Moulding Parameters

Parameter	Value
Melt temperature (°C)	400
Maximum injection velocity (mm/s)	750
Clamping force (kN)	50
Holding pressure (bars)	600
Mould temperature (°C)	210

20AHT auto sampler and SPD-M20A PDA detector was used for the analysis of the samples. Data acquisition was carried out using LC solutions software. Separation was achieved on an Agilent Eclipse column (150 × 4.6 mm; 5 μm). The mobile phase comprised of 0.02% *v/v* formic acid/methanol 75:25 (*v/v*) at a flow rate of 1 mL/min with an injection volume of 20 μL and the eluents were monitored at 221 nm. The developed method was validated as per ICH guidelines.

Solubility Studies

The solubility of RIZ was studied in different vehicle combinations of propylene glycol (PG), polyethylene glycol-400 (PEG) and saline at 70:30, 80:20 and 90:10% *v/v* ratios. To each vehicle system, excess amount of RIZ was added and vortexed for 1 min in order to obtain a saturated solution, and the solutions were equilibrated at 37°C in an orbital shaker for 24 h. After equilibration, the samples were centrifuged at 3000 rpm for 10 min and filtered through a nylon syringe filter (0.45 μm), and all the samples were appropriately diluted and analysed by the HPLC method.

Skin Preparation

Pig ears were collected from the local abattoirs immediately after animals were killed by electric current. The ears were transported to the laboratory in a cooling box without previous treatment. In the laboratory, the pig ears were washed carefully with distilled water and the hair was removed from the external part of pig ear using an electrical hair clipper. Carefully, the full-thickness skin from the external part of the pig ear was separated from the underlying cartilage using a scalpel, and excess fat underlying the skin was removed to a thickness of 1.2 mm which was employed for the *in vitro* transdermal permeation studies. The dermis side was wiped with isopropyl alcohol to remove the residual adhering fat. Processed skin samples were individually wrapped in plastic bags without air entrapment and stored in a deep freezer at −20°C till further use.

Table II. Brightness Switch Settings Used for the Confocal Measurements

Position (μm)	Brightness
600	49
550	47.1
520	49.1
20	75.5
0	48.4

Application of MNs on Skin Samples

Prior to the *in vitro* skin permeation experiments, the skin samples were kept at room temperature and then the skin surface was carefully washed with saline. Two types of MN devices *viz*. ADM (0.6, 0.9, 1.2 and 1.5 mm) and PM (0.6 mm) were tried to poke the skin surface under thumb pressure. In the case of PM, both single (PM-1) and triple (PM-3) insertions at different places within a 1.77-cm^2 skin area (PM-3) were made in order to maintain the MN density closer to ADM of 0.6 mm length as shown in Fig. 1. The MNs were periodically checked in between usage for potential damages of the needles under a stereomicroscope.

Surface Visualization and Histological Examination of the Skin Samples

To visually confirm the ability of disruption of skin layers by MNs, the arrays were pressed over the pig ear skin under thumb pressure and held for 1 min. Then, the skin was stained with safranin dye (1% *w/v* in water) and wiped with isopropanol cotton swabs for the identification of the microconduits formed. In the case of the histological studies, the skin section samples with and without MN treatments were prepared after staining with haematoxylin and eosin for visualization of skin layers and to display a clear indentation by MN penetration. The sections were observed under a microscope (Olympus; Noida, India). The width and depth of the microconduits formed were also calculated in triplicate ($n = 3$ skin samples for each MN) with the help of ToupView 3.2 Software (Irwin, USA). For the control, skin samples without MN treatment were also prepared.

In Vitro Skin Permeation Studies

The *in vitro* transdermal permeation studies were performed using a vertical type Franz diffusion cell apparatus fitted with a water circulation system, a water heater and an eight-stage magnetic stirrer (Orchid Scientifics, Nasik, India). Franz diffusion cells with an effective diffusion area of 1.77 cm^2 and a receptor volume of around 14 mL were used. Saline was used as the receptor fluid. Pig ear skin was mounted between the donor and receptor cells with SC facing towards the donor cell. The receptor medium was stirred for uniform drug distribution at a speed of 600 rpm throughout the experiment. Care was taken to prevent the entrapment of air bubbles underside of the skin (dermis) and receptor solution. The surface of the skin was maintained at 32°C using a circulating water bath. After equilibration, 500 μL of donor solutions containing excess amount of RIZ were applied on to the skin. Samples (500 μL) were withdrawn from the receptor fluid at 6-h increments up to 48 h and replaced with the fresh saline to maintain a constant volume. All the samples were stored at 4°C until analysed by HPLC.

The cumulative permeation profiles were plotted for the cumulative amount of drug permeated (nmol/cm^2) as a function of time, for untreated and microneedle-treated skin.

The flux values and the respective lag times were obtained from the slope and the X-intercept of the steady-state portion of the cumulative permeation profiles. Apparent permeability and diffusion coefficient values were computed from Fick's first law of diffusion:

$$\frac{1}{A}\left(\frac{dM}{dt}\right) = J_s = K_p \Delta C$$

J_s is the steady-state flux (nmol/cm^2/h), M is the cumulative amount of drug permeating the skin (nmol/cm^2), A is the area of the skin (1.77 cm^2), K_p is the apparent permeability coefficient (cm/h) and ΔC is the difference in concentrations of RIZ in the donor and receiver. Sink conditions were maintained in the receiver throughout the experiment, and hence, ΔC was approximated to the drug concentration in the donor compartment.

Enhancement ratios were also computed to evaluate the relative efficiency of different MNs on the RIZ skin permeation enhancement. The enhancement ratios were calculated as follows:

$$\text{Enhancement Ratio} = \frac{\text{Cumulative amount or Flux obtained after MN application}}{\text{Cumulative amount or Flux obtained from passive studies}}$$

RIZ Content in Skin

After the completion of the permeation studies, skin samples were studied for drug disposition. The skin tissue exposed to the donor solution was cut with a scalpel and washed with filtered water and blotted with a paper towel in order to remove the adhered drug to the surface. Then, the skin was minced with a scalpel and placed in a pre-weighed vial. The drug was extracted from the skin by equilibrating with 5 mL of acetonitrile at 32°C in an orbital shaker. The solutions were then analysed by HPLC to determine the RIZ content.

Scaling Analyses

Dimensionless correlations between the amount of RIZ permeated (C_t/C_s) and other variables like thickness (h/L) and surface area (S_a/L^2) of the skin were made in order to gain insights into the overall phenomenon of RIZ transdermal permeation enhancement by MN application. The scaling analyses were carried out based on the principles of Buckingham π theorem where it is defined that the dimensionless concentration of a drug, which permeates through skin, can be defined in terms of key non-dimensional parameters (*e.g.* MN lengths) using the procedures described in previous papers (17,18).

Equation 1 describes the relationship of all the model parameters used for such analyses (Table III).

$$\frac{C_t}{C_s} = K\left[\frac{S_a L^4 K_e}{V_d h D}\right]^n \quad (1)$$

Where K is a dimensionless constant and n is an unknown power; C_t and C_s are the amount of drug permeated at a given time t (48 h) and the amount of drug loaded in the donor compartment for diffusion (surface concentration on the skin); S_a is the surface area of the skin available for diffusion; L is the length of the microneedles; K_e and V_d are the first-order elimination constant and the volume of the receptor fluid; h is the thickness of the skin; and D is the diffusion coefficient of RIZ in skin.

Using Eq. 1, the correlations between the dimensionless RIZ concentration (C_t/C_s) against different dimensionless parameters of the study, h/L and S_a/L^2, have been established considering that all other variables remain unchanged.

Numerical Simulations of Experimental Studies

A set of well-defined numerical simulations were carried out in order to gain insights into the specific effects of MN shape, dimensions, force of insertion of MN, *etc.* on the overall permeation enhancement of RIZ, and also to obtain the information about RIZ distribution within the skin layers during permeation, which are otherwise difficult to obtain directly from the experimental data. The simulations were carried out using MATLAB (Math Works, MA, USA) and COMSOL Multiphysics (COMSOL Multiphysics Pvt. Ltd.,

Table III. Model Parameters for Dimensional Scaling Analyses of the Data

Parameter	Value
Duration for medication: t_m	48 h
Surface area of skin exposed: S_a	1.77 cm^2
Thickness of stratum corneum: h_{sc}	0.002 cm
Total thickness of membrane (distance to blood vessel): h	0.12 cm
Effective skin thickness: h_e	Variable
Diffusion coefficient in viable skin: D	Variable
Volume of fluid in receptor compartment (distribution): V_d	14 mL
Skin surface/donor concentration: C_s	Saturated solution was charged as the donor solution
Microneedle length: L	0.06, 0.09, 0.12 and 0.15 cm

Stockholm, Sweden) programs. The MATLAB program was used to process the histological section images of skin treated with MNs and these processed images were further coupled with the experimental permeation parameter, *e.g.* passive diffusion coefficient and imported into the COMSOL simulator software (18,19).

Statistical Analysis of the Data

Results of the experimental data were subjected to statistical analysis by one-way ANOVA (using Fischer's LSD *post hoc* test) using SYSTAT 13 software (Systat Software Inc., San Jose, USA). Results with p value of less than 0.05 were considered to have statistically significant variance. Mean of replicate measurements ($n = 3$) with corresponding standard deviation (SD) was used to represent the data and to plot the graphs.

RESULTS

Fabrication and Characterization of PM

PM arrays were fabricated using PEEK-LT-3 using the microinjection moulding technique, with 25 MN on each array (MN density) and an array base thickness of 300 μm. The dimensions of PM, determined using 3D confocal imaging (Fig. 3a) and scanning electron microscopy (SEM) (Fig. 3b), were found to be 556 ± 30 μm in height with a tip radius of 32 ± 8 μm, with a base thickness of 300 μm and MN interspacing of approximately 1 mm at the base.

For better comparison and understanding of the difference in the shape/design between PM and ADM devices, 3D confocal images of 0.6 mm ADM were given in Fig. 3c. Also the difference in base thickness among the

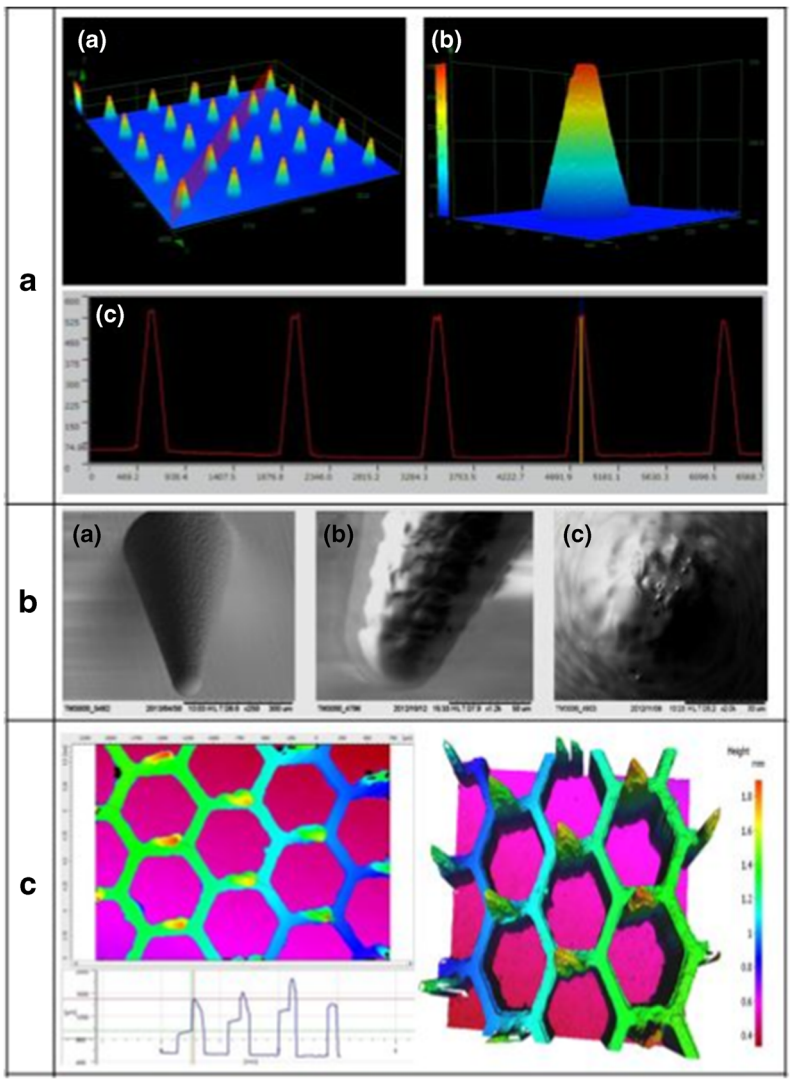

Fig. 3. **a** 3D confocal image of *a* front view of the PEEK MN array, *b* single MN of PEEK and *c* line measurement of the needle array. **b** SEM image of the PEEK MNs: *a* single needle ×250, *b* single needle ×1200 and *c* single needle ×2000. **c** Representative 3D confocal image of 0.6 ADM showing its design parameters

Table IV. Different Geometry Parameters of MNs Used in the Study

Parameter	ADM[a]				PM
	0.6	0.9	1.2	1.5	
Length (μm)	600	900	1200	1500	560 ± 30
Number of MNs (1.77 cm^2)	187	85	41	31	25
Shape	Flat (2D)				Conical (3D)
Thickness of each MN (μm)	78 (uniform till tip)[b]				300 (~30 at tip)
Thickness of array base (μm)	100–200[b]				300
Material	Medical grade stainless steel (SS 316L)				PEEK LT-3 (polyether ether ketone)

[a] Values are from the manufacturer (20)
[b] The width and thickness of the MN and the base vary with length

devices can be clearly observed from Fig. 1. The various geometry parameters of both types of MN devices are given in Table IV.

Analytical Method

A rapid and sensitive HPLC-PDA method was developed for the selective quantification of RIZ in transdermal permeation studies. Under the developed LC conditions, RIZ eluted at 2.5 min (Fig. 4a) with a good peak shape. Also, the specificity of the method to RIZ was demonstrated by the UV spectrum and the peak purity index curves (Fig. 4b, c). The method was validated as per ICH guidelines and complied with all the requirements (Table V).

Solubility Studies

Solubility studies for RIZ were performed with a view to select appropriate donor vehicle for conducting *in vitro* skin permeation studies. PG/saline and PEG/saline combinations at 70:30, 80:20 and 90:10% *v*/*v* were studied for RIZ solubility. The solubility data obtained is shown in Fig. 5.

Surface Visualization and Histological Examination of Skin Samples

The digital photographs of MN-treated skin are shown in Fig. 6. Histological section images of skin treated with MNs are shown in Fig. 7. From the images, the stratum corneum

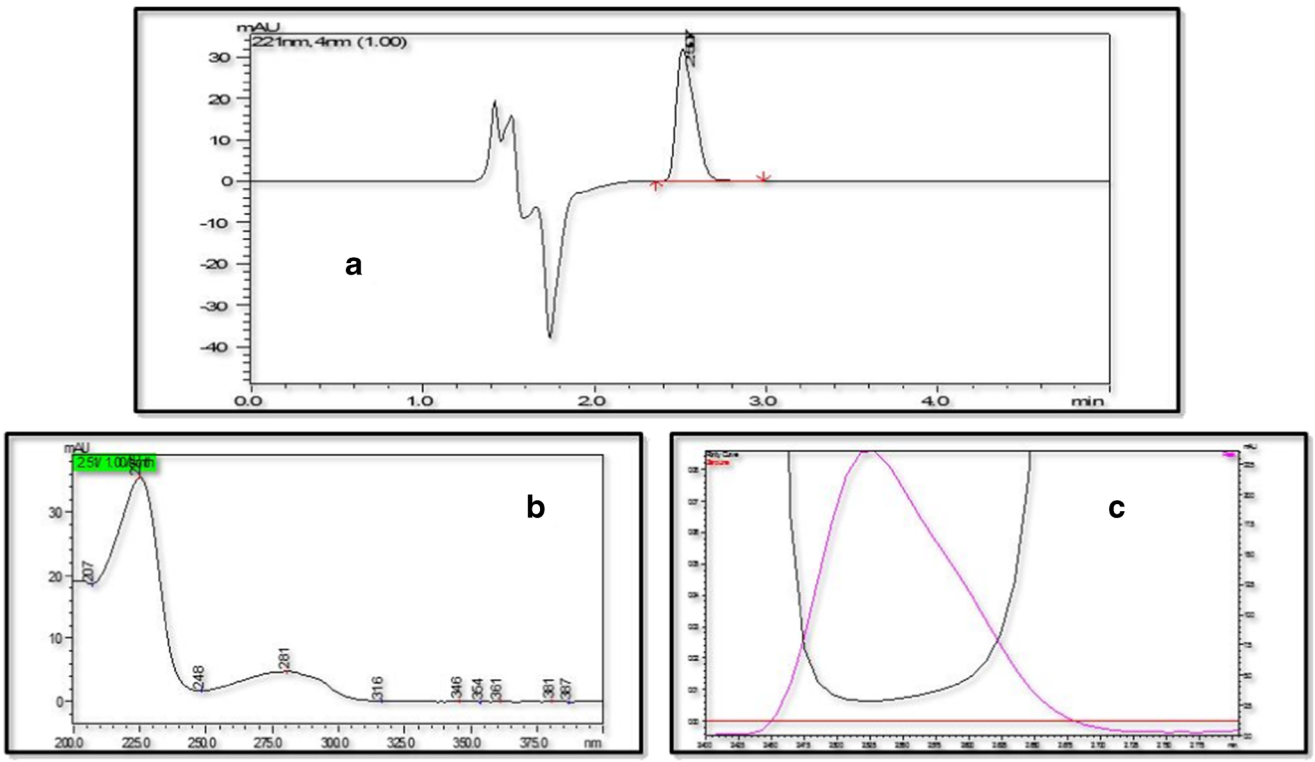

Fig. 4. RIZ chromatogram (**a**). UV spectrum (**b**). Peak purity index (**c**)

disruption and the formation of microconduits across skin layers were clearly evident. The average penetration depth (vertical) ($n = 3$) of the MNs was found to be 180.26 ± 30.39, 302.22 ± 22.28, 400.85 ± 20.83, 478.48 ± 67.72 and 338.20 ± 22.66 μm for ADM (0.6, 0.9, 1.2, 1.5 mm) and PM, respectively.

In Vitro Permeation Studies

The comparative *in vitro* pig ear skin permeation profiles of RIZ without and with MN application are shown in Fig. 8. Various RIZ permeation parameters *viz*. cumulative amount permeated at the end of 48 h, steady-state flux, lag time, permeability and diffusion coefficients without and with microneedle treatment are given in Table VI.

Scaling Analyses

Using scaling analyses, correlations were developed between the dimensionless parameters, namely, the amount of RIZ permeated (C_t/C_s) and skin thickness (h/L) and surface area of the skin (S_a/L^2) in order to derive a better understanding on the effect of specific geometry parameters of MN, like length (L), on overall permeation enhancement by MNs of same design (ADM) (Fig. 9a, b, respectively) (17,18). Equations 2 and 3 describe such relationships among the considered parameters within the given range. These correlations were determined for a given thickness and surface area of the skin while the MN length varies (0.6, 0.9, 1.2 and 1.5 mm).

$$\frac{C_t}{C_s} = 4.864 \times 10^{-3}\left[\frac{h}{L}\right]^{-1.592} \quad \text{for} \quad 0.8 \le \frac{h}{L} \le 2 \tag{2}$$

$$\frac{C_t}{C_s} = 0.224\left[\frac{S_a}{L^2}\right]^{-0.796} \quad \text{for} \quad 78.5 \le \frac{S_a}{L^2} \le 491.5 \tag{3}$$

A good correlation was observed ($R^2 > 0.85$) between the dimensionless parameters of the study (Fig. 9).

Numerical Simulations of Experimental Studies

The numerical simulations were carried out using the procedures discussed in previous papers based on *in vitro* passive diffusion coefficient values, coupled with histological section images (of corresponding MNs) (18,19). Different stages in processing the histological section images by MATLAB and COMSOL programs for simulations are shown in Fig. 10. The numerical simulations were able to provide information regarding the skin distribution of RIZ after applying the MNs at any time point and depth (Fig. 10d).

DISCUSSION

The shape (conical) and dimensions of the PM were found to be consistent and repeatable with good tip shape, confirming the complete filling of the PEEK into the MN insert cavity under the maintained processing conditions (Table I), and the technique used is reliable for the bulk manufacture of PMs. Moreover, compression tests of PM on a steel plate using Bose Electroforce 3100 instrument with a 225-N load cell and Wintest® software (Bose, MN, USA) revealed that the PMs were able to withstand compression forces of up to 8 N. Plastic deformation of the PMs was observed at forces greater than 16 N, with no tip breaking (16).

Table V. RIZ HPLC Validation Data

Linearity ($n = 3$)	
Range	0.2–3 μg/mL
Regression equation	$y = 78{,}500x - 418.87$
Correlation coefficient	$R = 0.999$
Regression coefficient	$R^2 = 0.999$
Precision ($n = 6$)	Average peak area of the standard sample (%RSD) 76,214 (0.529)
Accuracy ($n = 3$)	Mean percent recovery (%RSD)
% level of addition	
80	100.31 (0.685)
100	100.46 (0.34)
120	100.08 (0.980)

A rapid and sensitive HPLC-PDA method was developed for the selective quantification of RIZ in transdermal permeation studies (Fig. 4). The method complied with all the requirements of ICH guidelines (Table V) and was successfully employed for the quantitative estimation of RIZ in various samples throughout the study. The solubility of RIZ was in the order 70:30 > 80:20 > 90:10% *v/v* in both PG/saline and PEG/saline solvent systems. Overall, the solubility of RIZ was significantly higher in PG/saline 70:30% *v/v* combination when compared to others ($p < 0.05$) (Fig. 5). Hence, PG/saline 70:30% *v/v* combination was further selected as the donor vehicle in permeation studies.

Surface visualization of the MN-treated skin samples showed clear distinctions in the number of the microconduits formed as per the length and density of MNs in ADM and PM devices (Fig. 6). Histological section images clearly

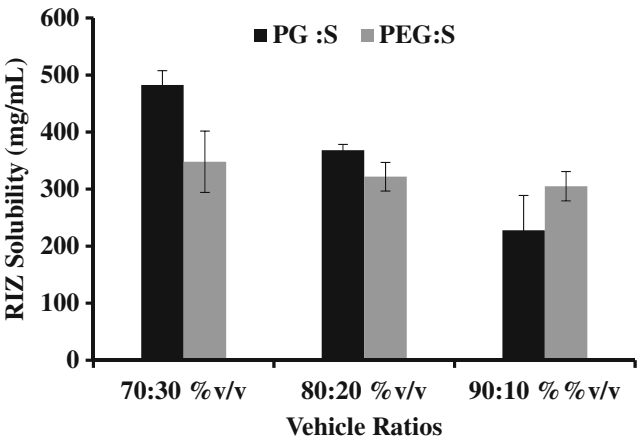

Fig. 5. Solubility data of RIZ in PG/saline and PEG/saline solvent systems

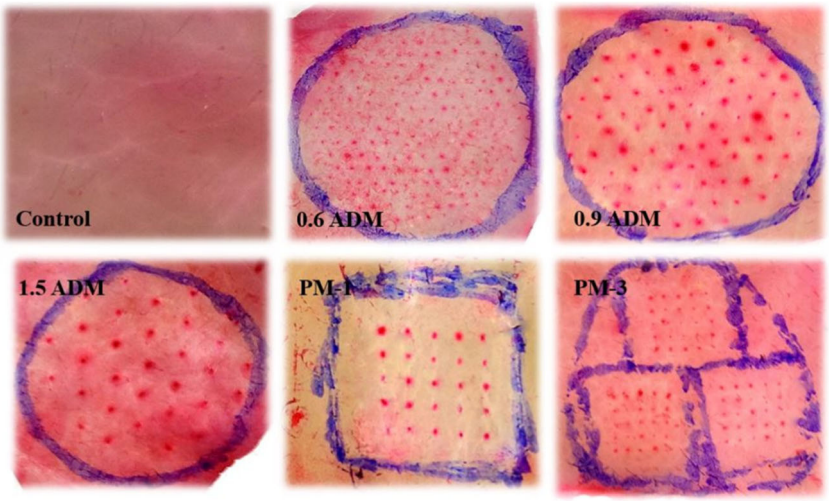

Fig. 6. Surface images of stained skin without and with MN treatment

showed skin layer disruption and the formation of microconduits (Fig. 7). The average penetration depth (vertical) was about 25–35% for ADM and 55–60% for the PM MN lengths (Fig. 7). Even though the length of the MNs differ in ADM, the percentage of MN penetration is almost the same, which is an indication of uniformity in thumb pressure under which MNs were applied at different times.

With the ADM devices, as the length of the MNs increased, the penetration depth also increased. However, the microconduits were found to be wider and deeper with PM when compared to ADM of similar lengths, *i.e.* 0.6 mm. These differences in the efficiency of creating microconduits in skin layers between the two types of MN devices (ADM and PM) may be attributed to the differences in geometry parameters like shape, design and type of fabricating material. Regarding the shape/design, PM being conical (3D) in shape, the microconduits formed by PM were wider, while that with ADM looks merely like a cut on the skin (2D) as the arrays of ADM are low in thickness (2D) (Fig. 3). Furthermore, owing to the sturdy and thick base (when

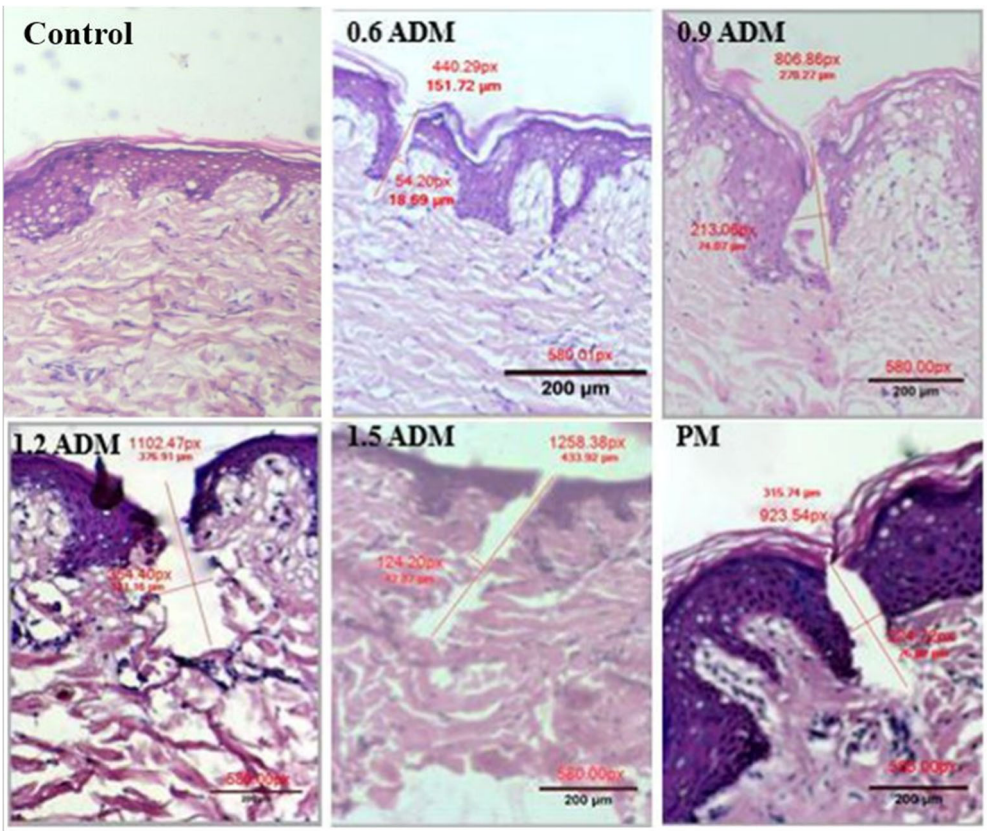

Fig. 7. Typical histological sections which were used for MN penetration depth calculation of ADM and PM in skin (ToupView® screenshot)

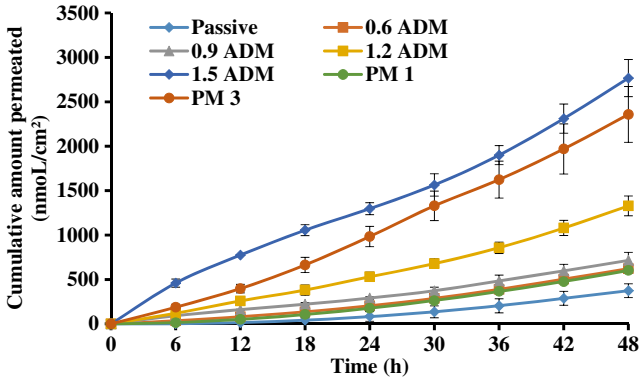

Fig. 8. Comparative *in vitro* skin permeation profiles of RIZ from passive and MN treatments

compared to ADM) that supports the solid PM (Fig. 1), the effective resistance (because of the viscoelastic nature) of the skin during application of arrays may be less for PM, while the ADM might have experienced greater resistance which is because of their thin base and array design (20), resulting in a relatively shallow penetration with similar MN lengths (0.6 and 0.9 mm ADM).

Significant enhancement in RIZ permeation was observed after MN application onto the skin ($p < 0.05$) when compared to passive permeation studies (Fig. 8). Increases of 1.76-, 1.91-, 3.55- and 7.41-fold in the cumulative amount (48 h) of RIZ permeated were observed with 0.6, 0.9, 1.2 and 1.5 mm ADM treatments, respectively, when compared to passive permeation amount. A similar trend was observed with other permeation parameters like permeability and diffusion coefficient values (Table VI). A significant reduction in lag time was observed after application of 1.5 mm ADM when compared to that with passive and other ADM lengths ($p < 0.05$). However, there is no statistically significant difference between passive and 0.6 mm and between 0.9 and 1.2 mm ADM treatments in terms of lag time ($p > 0.05$).

The RIZ flux values were found to be in the order of 1.5 mm > 1.2 mm > 0.9 mm > 0.6 mm > passive with ADM treatments. A 4.88-fold increase in RIZ flux was observed with the 1.5 mm when compared to passive studies. However, there is no statistically significant difference between 0.6 and 0.9 mm treatments ($p > 0.05$). It was observed that the enhancement of RIZ permeation was only marginal with the application of 0.6 and 0.9 mm ADM when compared to passive studies (Fig. 8). This may be due to the fact that the skin disruption/penetration caused by 0.6 and 0.9 mm ADM was less as supported by histological section images (Fig. 7).

Moreover, the RIZ permeation was high with 1.5 mm ADM when compared to 0.6, 0.9 and 1.2 mm even though the density of MNs is low, which may be because of longer needle lengths which in turn resulted in deeper skin penetration.

With the PM application, a 1.62- and 6.35-fold increase in the cumulative amount (48 h) of RIZ permeated was observed with PM-1 and PM-3 treatments, respectively, when compared to passive permeation amounts. The lag times were found to be significantly lower for PM-3 when compared to passive and PM-1 treatments ($p < 0.05$). The RIZ flux values were found to be in the order of PM-3 > PM-1 > passive treatments. A 4.52- and 1.49-fold increase in RIZ flux was observed with the PM-3 and PM-1, respectively, when compared to passive studies. A similar trend was observed with other permeation parameters like permeability and diffusion coefficient values (Table VI) with both PM treatments.

Even though the skin penetration by the PM device (with 0.6 mm array) was significantly greater when compared to 0.6 and 0.9 mm ADM, the overall permeation enhancement in terms of flux, cumulative amount permeated, *etc.* achieved with PM-1 was found to be closer to those of 0.6 and 0.9 mm ADM ($p > 0.05$). This may be because the needle density of 0.6 and 0.9 mm ADM was greater when compared to PM-1 (Table III), which may have compensated the variation in the extent of skin penetration among these MNs, and thus, no significant variation in overall permeation enhancement was observed among these three MNs ($p > 0.05$).

In case of the PM, a single application of array did not cover the 1.77-cm^2 surface area of the skin, and hence in order to maintain the MN density closer to ADM of 0.6 mm length, the arrays were applied three times at different places within a 1.77-cm^2 skin area (PM-3) as shown in Fig. 1. As the needle density was increased with PM-3, the RIZ transdermal permeation increased markedly and was similar to that obtained with 1.5 mm ADM ($p > 0.05$).

Moreover, it is intriguing to note that although the needle density PM-3 (75 MNs) was significantly greater when compared to 1.5 mm ADM (31 MNs), the overall RIZ permeation enhancement was considerably greater with

Table VI. Permeation Parameters of RIZ Without and With MN Treatments

Skin treatment	Permeation parameters					
	Cumulative amount permeated at 48 h (nmol/cm^2)	Steady-state flux (nmol/cm^2/h)	Lag time (h)	Permeability coefficient ($\times 10^{-05}$) (cm/h)	Diffusion coefficient ($\times 10^{-08}$) (cm^2/s)	Skin content (μg/g)
Passive	373.451 ± 77.524	12.648 ± 1.212	19.69 ± 4.73	2.271 ± 0.218	7.570 ± 0.726	794.30 ± 174.43
0.6 ADM	621.665 ± 46.356	18.664 ± 0.84	14.84 ± 1.96	3.348 ± 0.152	11.161 ± 0.507	1213.78 ± 361.77
0.9 ADM	715.246 ± 89.447	18.675 ± 2.825	9.98 ± 0.91	3.353 ± 0.507	11.178 ± 1.691	1200.94 ± 260.13
1.2 ADM	1328.277 ± 111.659	33.435 ± 3.182	9.87 ± 1.38	6.004 ± 0.571	20.012 ± 1.905	1015.54 ± 148.37
1.5 ADM	2767.532 ± 209.109	61.756 ± 4.260	4.17 ± 0.85	11.089 ± 0.756	36.963 ± 2.550	1566.92 ± 628.71
PM-1	602.023 ± 17.269	18.858 ± 1.35	16.31 ± 2.05	3.387 ± 0.243	11.29 ± 0.809	1247.31 ± 445.51
PM-3	2358.39 ± 314.393	57.199 ± 9.03	7.06 ± 1.61	10.273 ± 1.62	34.243 ± 5.406	1338.26 ± 345.97

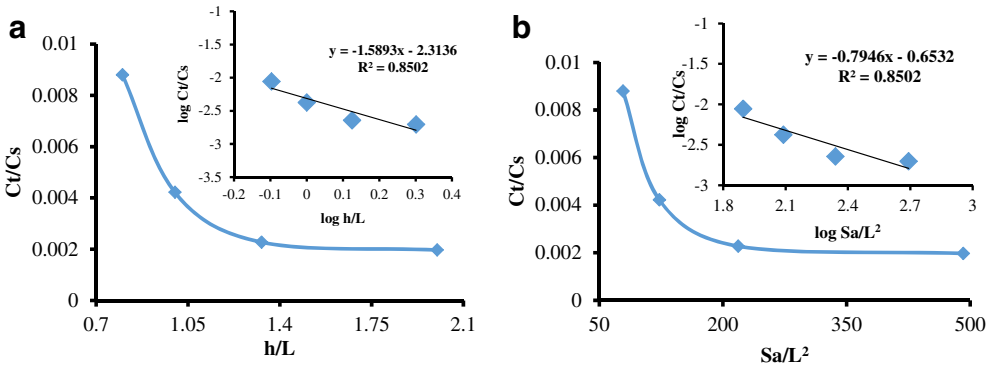

Fig. 9. Scaling relationship of different dimensionless groups for permeation of RIZ. **a** Effects of dimensionless length of microneedles. **b** Effects of dimensionless surface area for diffusion

1.5 mm ADM with significantly shorter lag times ($p < 0.05$), which may be because of deeper (vertical) penetration into the skin. Even though the depth of the penetration was significantly lower with PM when compared to 1.5 mm ADM, the comparable permeation enhancement by PM-3 may be because of higher needle density as stated earlier and wider microconduits formed as evidenced by histological section images (Fig. 7).

The enhancement in RIZ permeation was found to be in the order of 1.5 mm ADM ≥ PM-3 > 1.2 mm ADM > 0.9 mm ADM ≥ 0.6 mm ADM ≥ PM-1 > passive. Even though no correlation of RIZ skin content was observed with different MN treatments, significantly higher amounts of RIZ were found to be distributed in skin layers at the end of 48 h with MN-treated studies and are an indication of potential RIZ skin deposition.

Overall, transdermal permeation enhancement of RIZ by MN application is a complex phenomenon, and permeation enhancement is dependent on several aspects of the MN geometry like the shape/design, length, density, *etc.*

Dimensionless correlations were developed for ADM MNs (same type but differing in length) using scaling

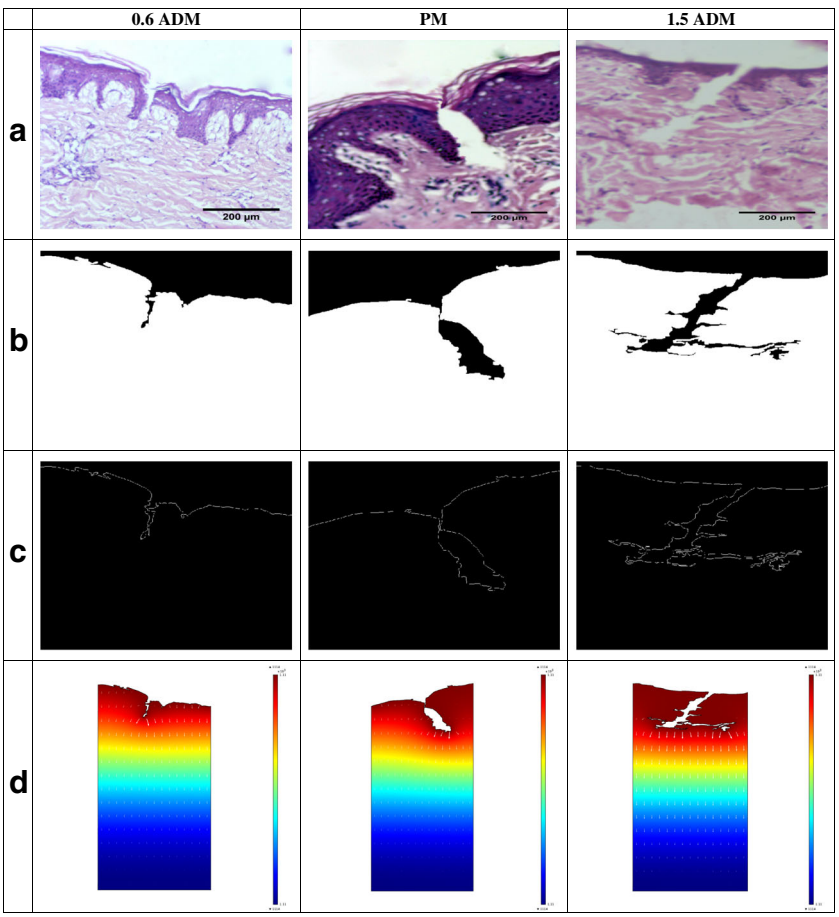

Fig. 10. **a** The histological section images of skin. **b**, **c** Images treated and processed with MATLAB program. **d** Drug distribution using images simulated in COMSOL

analyses. Good correlations were observed between the dimensionless parameters (C_t/C_s *vs* h/L and C_t/C_s *vs* S_a/L^2) (Fig. 9). These correlations can be used to predict the amount of RIZ permeated (C_t/C_s) with high accuracy for other MN lengths in the range of 0.6–1.5 mm with similar design as ADM.

From the results of numerical simulations, the flux was represented by white arrows in the figures (Fig. 10d) showing obvious increment at the upper layers of the skin which is caused by MN penetration. This increment may be extrapolated to a higher drug accumulation rate at the blood stream as well as shorter lag time for the diffusion to reach its steady state after the application of MNs. Based on the simulation results, the diffusion profile of RIZ showed significant permeation increment with 1.5 mm ADM and PM when compared to other MNs in the study. Furthermore, the advantage of greater penetration by PM can be further magnified by increasing the MN density, as in the case of PM-3.

These simulations can be of great research value as they may be used to predict the degree of transdermal permeation enhancement of RIZ with other (new) dimensions and designs of MNs using the respective histological section images and the passive diffusion coefficient data.

CONCLUSION

Two types of MN devices (ADM and PM) were employed in this investigation to derive a greater understanding on the effects of various geometry parameters specifically on the transdermal permeation of RIZ by MN application. It was observed that the application of MNs significantly enhance the transdermal permeation of RIZ across pig ear skin. Moreover, the type/shape, density, and more importantly, length of MNs (depth of penetration into the skin) were found to play a crucial role in the overall permeation enhancement of RIZ using this technique. It may be inferred that the transdermal delivery of RIZ, at clinically significant levels and in a painless and non-invasive manner, may by possible using MN application. This investigation can form the basis for further studies (*in vivo*) and for optimization of various MN parameters to achieve successful delivery of RIZ *via* MN-assisted transdermal delivery systems.

ACKNOWLEDGEMENTS

The authors are thankful to Mylan Pharmaceuticals India Ltd, Hyderabad, for providing a gift sample of RIZ; to Dr. Naveen, Department of Pathology, Dr. Pinnamaneni Siddhartha Institute of Medical Sciences and Research Foundation, Vijayawada, for providing the required facilities for taking histological sections of skin samples; and also to the Siddhartha Academy of General and Technical Education, Vijayawada, for providing the necessary facilities to carry out the research work. The authors also extend their sincere thanks to DST, Ministry of Science and Technology, Govt. of India, and the British Council, London, UK, for funding this research work under the DST-UKIERI scheme (DST/INT/UK/P-60/2014).

COMPLIANCE WITH ETHICAL STANDARDS

Conflict of Interest The authors declare that they have no conflict of interest.

REFERENCES

1. Brown MB, Gary PM, Stuart AJ, Franklin KA. Dermal and transdermal drug delivery systems: current and future prospects. Drug Deliv. 2006;13:175–87.
2. Prausnitz MR, Robert L. Transdermal drug delivery. Nat Biotechnol. 2008;26:1261–8.
3. Cheung K, Das DB. Microneedles for drug delivery: trends and progress. Drug Deliv. 2014;23:1–7.
4. Prausnitz MR, Samir M, Robert L. Current status and future potential of transdermal drug delivery. Nat Rev Drug Discov. 2004;3:115–24.
5. Ritesh K, Anil P. Modified transdermal technologies: breaking the barriers of drug permeation via the skin. Trop J Pharm Res. 2007;6:633–44.
6. Han T, Das DB. Potential of combined ultrasound and microneedles for enhanced transdermal drug permeation: a review. Eur J Pharm Biopharm. 2015;89:312–28.
7. Silberstein SD. Migraine symptoms: results of a survey of self-reported migraineurs. Headache. 1995;35:387–96.
8. Rapoport AM, Tepper SJ, Sheftell FD, Kung E, Bigal ME. Which triptan for which patient? Neurol Sci. 2006;27:S123–9.
9. Marcelo EB, Carlos AB, Ana LA, José G. The triptan formulations—a critical evaluation. Speciali Arq Neuropsiquiatr. 2003;61:313–20.
10. Gill HS, Denson DD, Burris BA, Prausnitz MR. Effect of microneedle design on pain in human volunteers. Clin J Pain. 2008;24:585–94.
11. Jeong W, Lee A, Jung-Hwan PB, Prausnitz MR. Dissolving microneedles for transdermal drug delivery. Biomaterials. 2008;29:2113–24.
12. Zhou CP, Liu YL, Wang HL, Zhang PX, Zhang JL. Transdermal delivery of insulin using microneedle rollers in vivo. Int J Pharm. 2010;39:127–33.
13. Nalluri BN, Sai Sri Anusha V, Bramhini SR, Amulya J, Sultana AS, Teja UC, *et al.* In vitro skin permeation enhancement of sumatriptan by microneedle application. Curr Drug Deliv. 2015;12:761–9.
14. Gomaa YA, Morrow DI, Garland MJ, Donnelly RF, El-Khordagui LK, Meidan VM. Effects of microneedle length, density, insertion time and multiple applications on human skin barrier function: assessments by transepidermal water loss. Toxicol In Vitro. 2010;24:1971–8.
15. Attia UM, Marsona S, Alcock JR. Micro-injection moulding of polymer microfluidic devices. Microfluid Nanofluid. 2009;7:1–28.
16. Nair KJ, Whiteside BR, Grant C, Patel R, Tuinea-Bobe C, Norris K, *et al.* Investigation of plasma treatment on micro-injection moulded microneedle for drug delivery. Pharmaceutics. 2015;7:471–85.
17. Al-Qallaf B, Das DB, Mori D, Cui Z. Modelling transdermal delivery of high molecular weight drugs from microneedle systems. Phil Trans R Soc A. 2007;365:2951–67.
18. Leeladurga V, Teja UC, Sultana SA, Sudeep K, Anusha VS, Han T, *et al.* Application of microneedle arrays for enhancement of transdermal permeation of insulin: in vitro experiments, scaling analyses and numerical simulations. AAPS PharmSciTech. 2015;29:1–8.
19. Han T, Das DB. A new paradigm for numerical simulation of microneedle-based drug delivery aided by histology of microneedle-pierced skin. J Pharm Sci. 2015;104:1993–2007.
20. Yuzhakov VV, Yuzhakov Vadim V. Microneedle array, patch, and applicator for transdermal drug delivery. United States Patent US 7,658,728. 2010.